Atmos. Meas. Tech. Discuss., 5, 7507–7533, 2012
www.atmos-meas-tech-discuss.net/5/7507/2012/
doi:10.5194/amtd-5-7507-2012

Atmospheric Measurement Techniques Discussions

Radar-radiometer retrievals of cloud number concentration and dispersion parameter in marine stratocumulus

J. Rémillard, P. Kollias, and W. Szyrmer

Department of Atmospheric and Oceanic Sciences, McGill University, Montreal, QC, Canada

Received: 26 September 2012 – Accepted: 1 October 2012 – Published: 16 October 2012

Correspondence to: J. Rémillard (jasmine.remillard@mail.mcgill.ca)

Published by Copernicus Publications on behalf of the European Geosciences Union.

Abstract

The retrieval of cloud microphysical properties from remote sensors is challenging. In the past, ground-based radar-radiometer measurements have been successfully used to retrieve the liquid water content profile in nondrizzling clouds but offer little constraint in retrieving other moments of the cloud particle size distribution (PSD). Here, a microphysical condensational model under steady-state supersaturation conditions is utilized to provide additional constraints to the well-established radar-radiometer retrieval techniques. The coupling of the model with the observations allows the retrieval of the three parameters of a lognormal PSD, with two of them being height-dependent. Two periods of stratocumulus from the Azores are used to evaluate the novel technique. The results appear reasonable: continental-like number concentrations are retrieved, in agreement with the drizzle-free cloud conditions. The cloud optical depth derived from the retrieved distributions compares well in magnitude and variability with the one derived independently from a narrow field of view zenith radiometer. Uncertainties coming from the measurements are propagated to the retrieved quantities to estimate their errors. In general, errors smaller than 20 % should be attainable for most parameters, demonstrating the added value of the new technique.

1 Introduction

Extensive sheets of stratus and stratocumulus clouds lie above the eastern boundary current upwelling regions over the world's oceans (Klein and Hartmann, 1993). Marine stratocumulus clouds play a critical role in the boundary layer dynamics and are a key component in the earth's radiation budget (Randall et al., 1984; Ramanathan et al., 1989; Bony and Dufresne, 2005). However, appreciable complexity and challenges are found on smaller space and time scales, including the cloud-scale (Stevens and Feingold, 2009). If all other parameters are fixed, an increased aerosol concentration may reduce cloud droplet sizes, and therefore increase cloud optical thickness (the *Twomey*

AMTD
5, 7507–7533, 2012

effect, Twomey, 1977). In turn, reduced cloud droplet sizes can lead to precipitation suppression and increase the cloud lifetime (the *Albrecht effect*, Albrecht, 1989). However, recent modelling studies have suggested that elevated cloud condensation nuclei concentrations can also affect entrainment of free tropospheric air in the marine boundary layer (e.g. Ackerman et al., 2004), thus leading to important feedbacks that include both key processes.

Providing observational constraints for these processes at the cloud-scale requires coordinated multi-synergistic, multi-platform measurements. In situ aircraft-based observations provide direct measurements of cloud thermodynamical and microphysical properties, but are temporally and spatially limited. Ground-based supersites (e.g. Ackerman and Stokes, 2003) offer the advantage of continuous, multi-instrument observations. Relating the ground-based measurements to the variables of interest requires the use of physical or statistical retrieval techniques (e.g. Turner et al., 2007). Here, we are concerned with the retrieval of microphysical properties of nondrizzling stratocumulus clouds where condensation in an updraft and evaporation due to cloud-top mixing are the key processes that determine the profile of cloud microphysical properties.

Several previous studies have focused on the retrieval of microphysical processes in marine stratocumulus (Frisch et al., 1995, 1998, 2002; Fox and Illingworth, 1997; Kato et al., 2001; Turner et al., 2007). Frisch et al. (1998) first introduced the combination of radar-radiometer measurements to retrieve the in-cloud profile of liquid water content. Drizzle occurrence limits the applicability of the technique, and either the use of a radar reflectivity threshold (e.g. Liu et al., 2008) or the absence of radar echoes below the cloud base is used to remove drizzling clouds. In the absence of radiometer measurements, a variety of regression-based power law relations between the radar reflectivity factor and the liquid water content have been proposed (Atlas, 1954; Sauvageot and Omar, 1987; Fox and Illingworth, 1997; Wang and Geerts, 2003; Sassen and Liao, 1996; Kogan et al., 2007). The review paper of Turner et al. (2007) shows the large differences among the state-of-the-art liquid water content retrievals in nonprecipitating thin liquid clouds. Cloud optical depth measurements have also been used to

AMTD
5, 7507–7533, 2012

constrain the microphysical retrievals in stratocumulus clouds (Dong et al., 1997; Mace and Sassen, 2000; Kim et al., 2008; McComiskey et al., 2009). More recently, Martucci and O'Dowd (2011) developed a new technique combining radar and lidar profiles.

A new retrieval method is developed here, building on the previous retrieval technique introduced by Frisch et al. (1995, 1998, hereafter F95+) that used the combination of radar and radiometer measurements. Assuming that condensation and evaporation are the only processes controlling the evolution of the cloud particle size distribution (PSD), the vertical gradient of the attenuation-corrected radar reflectivity is used to derive the dispersion parameter (σ, assumed constant in the column) and the number concentration (N_{cld}, allowed to vary vertically around the derived column-averaged value). The observed mean Doppler velocity is used as a proxy for the vertical air motion, and it is used to estimate the supersaturation in the cloud.

This paper first briefly describes the typical instruments available. The novel approach is then described and illustrated by a couple of examples from the Azores. Finally, the results are compared to another instrument's measurements, to assess the feasibility of this technique.

2 Observations

The study utilizes marine stratocumulus observations collected during the recent deployment of the US Department of Energy Atmospheric Radiation Measurement (ARM) Mobile Facility (AMF) on Graciosa Island, Azores, in the context of the Clouds, Aerosol and Precipitation in the Marine Boundary Layer (CAP-MBL) field campaign. CAP-MBL took place from April 2009 to December 2010 in the Azores, to collect data on the physical and radiative properties of low-level clouds. The analysis is limited to low-level nonprecipitating marine stratocumulus clouds in the absence of other clouds, especially those containing liquid particles (e.g. cumulus).

Measurements from the W-band ARM Cloud Radar (WACR), two 2-channel microwave radiometers (MWR), the ceilometer, and the 2-channel Narrow Field of View

AMTD
5, 7507–7533, 2012

Zenith Radiometer (NFOV) are used in this study (Table 1). Time series measurements of column-integrated amounts of water vapour (the precipitable water vapour, PWV) and liquid water (the liquid water path, LWP) are provided from the MWRs. The uncertainty in the MWR-retrieved LWP is typically better than $20\,\mathrm{g\,m^{-2}}$, depending on the retrieval method (Turner et al., 2007). Cloud optical depth τ measurements are available from the NFOV at 1-s resolution (Chiu et al., 2006). Subsequently, the column-integrated cloud effective radius r_e can be estimated from τ_{NFOV} and LWP (e.g. Wood and Hartmann, 2006) using the expression $r_e = 9\mathrm{LWP}/(5\rho_w\tau_{NFOV})$. The ceilometer provides estimates of the cloud base height, and it is used in conjunction with the WACR data to ensure that the selected period contains no significant drizzle (i.e. WACR echoes below the cloud base).

The WACR provides information on the vertical structure of the marine stratocumulus clouds as depicted by the radar reflectivity (Z) and mean Doppler velocity (V_d) measurements. The WACR reflectivity profile is corrected for attenuation from water vapour and liquid water (e.g. Meneghini, 1978; Matrosov et al., 2004). The MWR provides the PWV and LWP measurements required for the estimation of the water attenuations. The vapour is distributed exponentially in the column, according to the surface pressure and temperature, while the liquid is distributed in the cloud layer using the Frisch et al. (1998) method. Information on temperature and pressure is obtained from the Balloon-Borne Sounding System (BBSS), which provides vertical profiles of both the thermodynamic state of the atmosphere, and the wind speed and direction. Water vapour and liquid water can produce a total two-way attenuation of 1–2 dB each, but oxygen attenuation remains negligible.

3 Retrieval method

Typically, an analytical form is chosen to represent the cloud PSD such that its moments depend only on three parameters: a characteristic size, a dispersion parameter, and

AMTD
5, 7507–7533, 2012

a concentration parameter. One of the widely used forms is the lognormal PSD:

$$n(r) = \frac{N_{\mathrm{cld}}}{\sqrt{2\pi}\sigma r} \exp\left(\frac{-(\ln r - \ln r_0)^2}{2\sigma^2}\right), \quad (1)$$

where r is the droplet's radius, N_{cld} the number concentration, r_0 the median radius, and σ the lognormal width (a measure of the PSD dispersion). Such a PSD form yields the following kth moment (see F95+):

$$\int r^k n(r)\,\mathrm{d}r = N_{\mathrm{cld}} r_0^k \exp\left(\frac{k^2}{2}\sigma^2\right). \quad (2)$$

The bulk quantities of distribution that represent physical quantities of interest are directly related to the moments of the cloud PSD. For instance, the liquid water content (LWC) relates to the third moment of the PSD, resulting in the following:

$$Q_{\mathrm{c}} = \frac{4\pi\rho_{\mathrm{w}}}{3}\int r^3 n(r)\,\mathrm{d}r = \frac{4\pi\rho_{\mathrm{w}}}{3} N_{\mathrm{cld}} r_0^3 \exp\left(\frac{9}{2}\sigma^2\right), \quad (3)$$

where ρ_{w} is the water density. The radar reflectivity factor (Z) is proportional to the backscattering cross-section of the droplets, which in turn relates to the sixth moment of the PSD since droplets are much smaller than the radar wavelength. Therefore, Z can be written as:

$$Z = 2^6 \int r^6 n(r)\,\mathrm{d}r = 2^6 N_{\mathrm{cld}} r_0^6 \exp\left(18\sigma^2\right). \quad (4)$$

Combining Eqs. (3) and (4), the dependence on one of the PSD parameters can be removed:

$$Q_{\mathrm{c}} = \frac{\pi\rho_{\mathrm{w}}}{6} \frac{\sqrt{N_{\mathrm{cld}} Z}}{\exp\left(\frac{9}{2}\sigma^2\right)}. \quad (5)$$

AMTD
5, 7507–7533, 2012

The application of Eq. (5) requires that either drizzle particles are absent or their presence does not affect the radar reflectivity profile. Alternatively, a separation of the measured Z values into their cloud and drizzle parts would be sufficient.

Analysis of a large database of in situ measurements taken in marine stratocumulus clouds suggests that the cloud concentration number and dispersion parameter are approximately constant with height (e.g. Miles et al., 2000). Based on these observations, most aforementioned retrievals algorithms also treat these two variables as invariant with height (e.g. Frisch et al., 1998). However, the vertical resolution of in situ measurements is usually coarse. Here, we only assume that σ is constant with height, and its value is estimated from the calculated column-averaged number concentration. To find that last quantity, we require that the variations of N_{cld} around its column average remain small (see below).

Integrating Eq. (5) throughout the cloud layer provides an equation for the LWP:

$$\mathrm{LWP} = \frac{\pi \rho_{\mathrm{w}}}{6} \frac{\langle N_{\mathrm{cld}}^{1/2} \rangle}{\exp\left(\frac{9}{2}\sigma^2\right)} \int \sqrt{Z(z)}\,\mathrm{d}z, \tag{6}$$

where the angled brackets represent a column averaging, weighted by the square-root of reflectivity: $\langle N_{\mathrm{cld}}^{1/2} \rangle = \int \sqrt{N_{\mathrm{cld}}(z)}\sqrt{Z(z)}\,\mathrm{d}z / \int \sqrt{Z(z)}\,\mathrm{d}z$. With LWP measurements available from the MWR, inverting Eq. (6) allows the retrieval of a column-averaged N_{cld}, albeit normalized by a function of the PSD dispersion:

$$N_{\mathrm{norm}}^{1/2} \equiv \frac{\langle N_{\mathrm{cld}}^{1/2} \rangle}{\exp\left(\frac{9}{2}\sigma^2\right)} = \frac{6\mathrm{LWP}}{\pi \rho_{\mathrm{w}} \int \sqrt{Z(z)}\,\mathrm{d}z}. \tag{7}$$

The derivation of the last relation is the same as in Frisch et al. (1998), but with the column-constant N_{cld} replaced with the column-averaged value $\langle N_{\mathrm{cld}}^{1/2} \rangle$.

In order to estimate the N_{cld} at a given height from the calculated $N_{\mathrm{norm}}^{1/2}$ in Eq. (7), we use the profile of vertical gradient of reflectivity. The vertical changes of reflectivity have

AMTD
5, 7507–7533, 2012

to reflect the evolution of PSD via active microphysical processes. In the absence of precipitation processes, the cloud droplets are assumed to grow only by condensation (and evaporation) as they follow the air motions. As such, the changes in reflectivity values are simply linked to the condensation/evaporation process, and the particle size growth rate is described by the following equation (e.g. Rogers and Yau, 1989):

$$\frac{\mathrm{d}r}{\mathrm{d}t} = \frac{S - \frac{a}{r} + \frac{b}{r^3}}{r\,[F_\mathrm{k} + F_\mathrm{D}]}, \tag{8}$$

where t is the time, S is the degree of saturation, a and b are constants depending on the curvature and solute of the droplet respectively, and F_k and F_D are atmospheric factors accounting for the thermal and diffusion effects respectively. Once initial droplets are formed, the curvature and solute terms can usually be neglected, leaving a simple form for the droplet's growth (and evaporation if $S < 0$). The time coordinate here relates to the height coordinate (z) through the vertical air motion (w_air), as cloud droplets sizes remain small enough to produce only negligible fall speeds. Equation (8) thus becomes:

$$\frac{\mathrm{d}r}{\mathrm{d}z} = \frac{S}{r w_\mathrm{air}\,[F_\mathrm{k} + F_\mathrm{D}]}. \tag{9}$$

On the other hand, the radar reflectivity factor is given by Eq. (4). In its most common units (dBZ), the reflectivity changes with height can then be written as:

$$\frac{\mathrm{d}(\mathrm{dBZ})}{\mathrm{d}z} = \frac{4.34}{Z}\frac{\mathrm{d}Z}{\mathrm{d}z} = \frac{4.34}{\int r^6 n(r)\,\mathrm{d}r}\int 6r^5 \frac{\mathrm{d}r}{\mathrm{d}z} n(r)\,\mathrm{d}r. \tag{10}$$

Using Eq. (9) for the change of radius with height, we get:

$$\frac{\mathrm{d}(\mathrm{dBZ})}{\mathrm{d}z} = \frac{26.04S}{w_\mathrm{air}\,[F_\mathrm{k} + F_\mathrm{D}]}\frac{\int r^4(r) n(r)\,\mathrm{d}r}{\int r^6 n(r)\,\mathrm{d}r} = \frac{26.04S}{w_\mathrm{air}\,[F_\mathrm{k} + F_\mathrm{D}]}\frac{1}{r_0^2 \exp\left(10\sigma^2\right)}, \tag{11}$$

AMTD
5, 7507–7533, 2012

where a lognormal PSD has been used to estimate the integrals (see Eq. 2).

Finally, it is assumed that steady-state conditions are reached and maintained inside the cloud (excluding the edges). Therefore, a steady-state supersaturation will be used, as derived by Korolev and Mazin (2003):

$$S_{qs} = \frac{a_0 w_{air}[F_k + F_D]}{b_0 \int r n(r)\,dr} = \frac{a_0 w_{air}[F_k + F_D]}{b_0 N_{cld} r_0 \exp\left(\sigma^2/2\right)}, \quad (12)$$

where a_0 and b_0 are variables depending on temperature and pressure (defined by Korolev and Mazin (2003), and summarized in Appendix Table A1). A lognormal PSD was assumed to obtain the right-hand side. Korolev and Mazin (2003) argued that this steady-state approximation holds in stratocumulus clouds, except near the edges. Solving for the ratio S_{qs}/w_{air} in Eq. (12), and substituting it into Eq. (11), the relation for the reflectivity gradient becomes:

$$\frac{d(dBZ)}{dz} = \frac{26.04 a_0}{b_0 N_{cld} r_0^3 \exp\left(\frac{21}{2}\sigma^2\right)}. \quad (13)$$

Notice that a dependence on the LWC appears in Eq. (13), although there is still a dependence on the dispersion parameter. Using Eqs. (4) and (7), the following relation is obtained:

$$\left[\frac{N_{cld}(z)}{\langle N_{cld}^{1/2}\rangle^2}\right]^{1/2} = \left\{\frac{208.32 a_0 N_{norm}^{1/6}}{b_0 \sqrt{Z(z)}}\left[\frac{d(dBZ)}{dz}\right]^{-1}\right\}\langle N_{cld}^{1/2}\rangle^{-4/3}. \quad (14)$$

On the right-hand side, all variables measured or obtained from measurements are grouped inside the braces.

Equation (14) still has two unknowns, but we can request that the profile of N_{cld} remains close to its column-averaged value, such that we search for the value of $\langle N_{cld}^{1/2}\rangle$

AMTD
5, 7507–7533, 2012

that minimizes the following integral:

$$\int \left| \sqrt{\frac{N_{\mathrm{cld}}(z)}{\langle N_{\mathrm{cld}} \rangle}} - 1 \right| \mathrm{d}z = \int \left| \left\{ \frac{208.32 a_0 N_{\mathrm{norm}}^{1/6}}{b_0 \sqrt{Z(z)}} \left[\frac{\mathrm{d}(\mathrm{dBZ})}{\mathrm{d}z} \right]^{-1} \right\} \langle N_{\mathrm{cld}}^{1/2} \rangle^{-4/3} - 1 \right| \mathrm{d}z. \quad (15)$$

Note that, as mentioned earlier, some assumptions are not valid at the edges. Therefore, the integral here excludes these radar volumes. Nevertheless, the retrieved column-averaged N_{cld} is assumed to apply also to the rogue volumes such that the remaining of the approach can still be done. Note however that mixing is considered above the reflectivity maximum in each profile, reducing the number concentration there by a factor equal to the square-root of the reflectivity ratio $Z(z)/Z(z_{\mathrm{max}})$.

Once a value is retrieved for $\langle N_{\mathrm{cld}}^{1/2} \rangle$ the three PSD parameters follow from Eq. (14) (for $N_{\mathrm{cld}}(z)$), Eq. (7) (for σ), and Eq. (4) (for $r_0(z)$). Then, the effective radius at each range gate can be calculated from:

$$r_{\mathrm{e}} = \frac{\int r^3 n(r)\,\mathrm{d}r}{\int r^2 n(r)\,\mathrm{d}r} = r_0 \exp\left(\frac{5}{2}\sigma^2\right). \quad (16)$$

By definition, the optical depth (τ) depends on the cloud PSD and the particles extinction cross-sectional area. For spherical droplets following a lognormal PSD with a column-constant width, τ in the visible light spectrum can be written as:

$$\tau = \int\int 2\pi r^2 n(r)\,\mathrm{d}r\,\mathrm{d}z = 2\pi \exp\left(2\sigma^2\right) \int N_{\mathrm{cld}}(z) r_0^2(z)\,\mathrm{d}z. \quad (17)$$

The retrieved τ will be compared with the optical depth independently derived from the measurements obtained by the collocated NFOV (Chiu et al., 2006).

AMTD
5, 7507–7533, 2012

4 Results

The method described above assumes that only cloud droplets contribute to the measurements. However, marine stratocumulus clouds have a propensity to produce drizzle, and it was observed that drizzle particles are nearly always present to some degree (Kollias et al., 2011). Therefore, the method is applied here to two periods when drizzle was rarely detected under the ceilometer cloud base, both observed on Graciosa Island, in the Azores, during June 2010. It is believed that the drizzle contributions to the WACR measurements in those cases are minimal, and are thus neglected here to demonstrate the possibilities of the new method. Its further application however requires the removal of the drizzle contribution to the measurements (Luke and Kollias, 2012).

4.1 Case of 13 June 2010

The first case is a stratocumulus cloud observed on 13 June 2010. Observed and retrieved parameters are shown for a two-hour daytime period (09:30–11:30 UTC; NFOV retrievals are available only during the day). No other cloud layer was observed during that period (e.g. cumulus or cirrus), and no significant drizzle was falling from the stratocumulus (Fig. 1a). The radar reflectivity profile peaks near the cloud top, further supporting either the lack of drizzle particles or their negligible role in the WACR moments. The Doppler measurements (Fig. 1b) show many short-lived up and down movements going through the cloud, with amplitudes typically smaller than $1\,\mathrm{m\,s^{-1}}$. Near the end of the two-hour period, downdrafts became more dominant, and a thinning of the cloud is visible through the rising of the cloud base. Eventually the cloud dissipated in the afternoon. Overall, the cloud had a depth of 200–250 m, with stable levels of LWP and PWV (Fig. 1c).

The retrieved column-averaged number concentration $\langle N_{\mathrm{cld}} \rangle$, the height-dependent N_{cld}, the column constant σ, and the height-dependent r_{e} and S_{qs} are shown in Fig. 2. Relatively high cloud droplet number concentrations are retrieved (N_{cld} between 400

AMTD
5, 7507–7533, 2012

and 600 cm^{-3}) with correspondingly small effective radius (r_e around 6 µm). Such values are typically found in continental stratocumulus clouds (Miles et al., 2000). Graciosa is an inhabited island and the air masses have origins with variable aerosol loadings (Rémillard et al., 2012). The lack of drizzle observations is consistent with the large retrieved number concentrations.

The retrieved σ values are varying between 0.2 and 0.4 (Fig. 2c). These values are in agreement with previous data sets, as reported by Miles et al. (2000), although in the lower half of the climatological estimated range. The low retrieved values of σ are consistent with the suggestion that the cloud droplets did not grow to drizzle sizes, keeping the PSD narrow. The supersaturation is estimated using Eq. (12). The WACR Doppler velocity measurements are assumed to represent well w_{air}, as no significant drizzle was detected and cloud droplets have fall velocities smaller than the radar resolution (a few $cm\,s^{-1}$). The resulting S_{qs} field has values within 0.1 % (see Fig. 2e). The S_{qs} retrieved field seems reasonable, although very few in situ measurements are available to compare.

Using Eq. (17), the cloud optical depth τ is retrieved and compared with the optical depth τ_{NFOV} retrieved from the NFOV measurements (Fig. 3a). The two independently retrieved optical depths agree very well, both in scales of variability and magnitude. Since the LWP variability drives to a large extent the τ variability, it is not surprising that the radar-radiometer derived and the shortwave derived optical depths agree in the observed scales of variability. Thus, the fact that the two retrievals exhibit very similar values ($\langle\tau\rangle - \langle\tau_{NFOV}\rangle = -0.5$) suggests that the proposed method retrieves the cloud microphysical parameters with reasonable accuracy. In particular, the slope of the relationship between cloud optical depth and LWP depends on the cloud effective radius (e.g. Kim et al., 2003). The linear regression of τ on the LWP values (Fig. 3d, e) shows very good fits, with similar slopes. The τ_{NFOV}–LWP derived effective radius retrievals exhibit larger variability compared to the effective radius retrieved using the radar-radiometer method (Fig. 3b). This different variability might come from the instruments sensitivities. The radar signal is most sensitive to variations in the presence

AMTD
5, 7507–7533, 2012

of big particles, while the effective radius is more affected by the small sizes of the PSD. Also, the assumption that σ is constant with height might also have impacted the variability of our retrievals, since the LWC and τ follow different relations with σ.

If the F95+ radar-radiometer based retrieval technique is applied to derive the cloud layer-average effective radius and optical depth, the range of solutions is very large, depending on the assumed cloud dispersion parameter value (see the grey shaded and hatched regions in Fig. 3).

Uncertainties on the retrievals have been evaluated by propagating an estimated error on each initial measurement: 1 K in the temperature field, 1 hPa in the pressure field, 1 dB for the corrected reflectivity field, and around 6 $\mathrm{g\,m^{-2}}$ for the LWP. The last one comes directly from the LWP retrieval (the physical method here), while the other values were chosen for illustration purpose. The uncertainty obtained from each instrument for the optical depth is shown in Fig. 3c. The main factor here is the radar reflectivity errors, due to its additive character in the equations. It results in bigger uncertainties for the deeper parts of the cloud, as more radar errors get added in the column.

Overall, the uncertainty shown here is close to the range of values obtained by the F95+ technique only by varying the lognormal width, without adding the instruments errors. It shows that the proposed method does constrain the retrieval parameter space. In fact, the uncertainty on the retrieved lognormal width and median radius is typically better than 20 % of the retrieved value when using the errors cited above.

4.2 Case of 29 June 2010

The second case is a stratocumulus cloud observed on the morning of 29 June 2010 (see Fig. 4) following nighttime drizzling conditions over the AMF location. Observed and retrieved parameters are shown for a two-hour daytime period (09:30–11:30 UTC). A thin cirrus layer (thickness from 0.5 to 1 km) is observed after 10:00 UTC at an altitude of 10 km. Very low intensity drizzle (−40 dBZ) is observed sporadically below the cloud base between 10:45 and 11:15 UTC (Fig. 4a). The radar reflectivity profile peaks near

AMTD
5, 7507–7533, 2012

the cloud top and exhibits values higher than those observed on the 13 June case. The Doppler measurements (Fig. 4b) show several coherent updraft and downdraft structures with vertical air motion magnitudes up to 1.5 m s^{-1}. Overall, the cloud has a depth of 250–350 m, with a peak in the LWP during the thickest cloud period (Fig. 4c).

The retrieved column-averaged number concentration $\langle N_{cld} \rangle$, the height-dependent N_{cld}, the column constant σ, and the height-dependent r_e and S_{qs} are shown in Fig. 5. Lower cloud droplet number concentrations are retrieved (N_{cld} between 200 and 400 cm^{-3}) with the effective radius reaching values up to 10 µm near the cloud top (Fig. 5a, b, d). As in the first case, the retrieved σ values are varying between 0.2 and 0.4 (Fig. 5c) and the supersaturation S_{qs} field has values within 0.1 % (Fig. 5e). However, it is clear in this case that more cloud area experienced higher supersaturation compared to the first case.

Once again, using Eq. (17), the cloud optical depth τ is retrieved and compared with the optical depth τ_{NFOV} retrieved from the NFOV measurements (Fig. 6a). The two independently retrieved optical depths agree very well, both in scales of variability and magnitude, although the bias is higher this time ($\langle \tau \rangle - \langle \tau_{NFOV} \rangle = -3$). The presence of the cirrus layer during the observing period provides a plausible explanation for the higher NFOV optical depth values. The linear regression of τ on the LWP values (Fig. 6d, e) shows very good fits, with similar slopes. As in the first case, the τ_{NFOV}–LWP derived effective radius retrievals exhibit larger variability compared to the effective radius retrieved using the radar-radiometer method (Fig. 6b).

An estimate of the uncertainties of the retrieved optical depths is shown in Fig. 6c. For this case, the statistical LWP retrieval was used instead of the physical one, providing a larger error (20 g m^{-2}). Consequently, it becomes the most important factor for the thin parts of the cloud.

AMTD
5, 7507–7533, 2012

5 Summary

Nonprecipitating liquid phase boundary layer clouds are an important component of the earth's energy budget. Ground-based cloud radars are capable of observing their vertical structure, dynamics and boundaries (Kollias et al., 2007). However, the use of the radar observables for the retrieval of microphysical parameters is limited to the use of the radar reflectivity as the sixth moment of the cloud PSD. Empirical or theoretical relationships have been proposed to relate the radar reflectivity to the third moment of the PSD, i.e. the LWC. This is the category of radar-only based algorithms. If LWP measurements from a microwave radiometer are available, the radar reflectivity factor can be used as a weighting function to distribute the LWP in the cloud column and thus retrieve the LWC profile with reasonable uncertainty (Frisch et al., 2000). This is the category of radar-radiometer based algorithms. Using additional constraints (e.g. number concentration and cloud dispersion parameter constant with height, or assuming a climatological value for the dispersion parameter), the cloud effective radius profile can be retrieved, and subsequently all other moments of the cloud PSD. However, these retrievals are subject to large uncertainties and generally do not agree with independent measurements of optical depth and/or solar transmission ratio (Dong et al., 1997; Mace and Sassen, 2000).

Here, a radar-radiometer based algorithm is proposed that is a considerable modification of the F95+ work. The proposed algorithm uses additional information from the radar observables to help to constrain the retrieval of cloud PSD parameters. A cloud condensational model is used to describe the profile of the radar reflectivity. It is demonstrated that the vertical gradient of the radar reflectivity combined with the steady-state supersaturation expression proposed by Korolev and Mazin (2003) can be used to constrain the relationship between cloud number concentration and dispersion parameter. Consequently, we only assume that σ is constant with height, and we keep the cloud number concentration height-dependent. However, it is required that variations of N_{cld} around its column average remain small. Moreover, the mean Doppler velocity is an

AMTD
5, 7507–7533, 2012

estimator of the vertical air motion, and it is used to estimate the cloud supersaturation using the relationship proposed by Korolev and Mazin (2003).

Observations from the recent deployment of the AMF on Graciosa Island are used to demonstrate the application of the technique in two nonprecipitating stratocumulus cloud examples. The new retrieval algorithm outputs profiles of effective radius, cloud number concentration, and supersaturation, and column values of cloud dispersion parameter. The temporal and spatial structures and magnitude of the retrieved parameters appear reasonable. However, without in situ observations, it is challenging to assess their accuracy.

Using the retrieved cloud PSD parameters, the cloud optical depth is estimated (Eq. 17) and compared to the retrieved optical depth from the NFOV radiometer (Chiu et al., 2006). In both cases, the comparison between the two optical depth estimates is very good. In the first case, the difference between the time-averaged optical depths ($\langle\tau\rangle - \langle\tau_{\mathrm{NFOV}}\rangle$) is better than −0.5. In the second case, the difference is greater (−3) however; the presence of a thin cirrus layer could explain the higher estimates of optical depth from the NFOV radiometer. Compared to the range of solutions using the F95+ technique, the proposed method clearly reduces the uncertainty in the estimation of the cloud effective radius and column-averaged dispersion parameter. This illustrates that, under certain conditions, the modelling of cloud and precipitation processes can help in the utilization of additional information hidden in radar observations.

References

Ackerman, A. S., Kirkpatrick, M. P., Stevens, D. E., and Toon, O. B.: The impact of humidity above stratiform clouds on indirect aerosol climate forcing, Nature, 432, 1014–1017, doi:10.1038/nature03174, 2004. 7509

Ackerman, T. P. and Stokes, G. M.: The atmospheric radiation measurement program, Phys. Today, 56, 38–44, doi:10.1063/1.1554135, 2003. 7509

Albrecht, B. A.: Aerosols, cloud microphysics, and fractional cloudiness, Science, 245, 1227–1230, doi:10.1126/science.245.4923.1227, 1989. 7509

AMTD
5, 7507–7533, 2012

Atlas, D.: The estimation of cloud parameters by radar, J. Meteorol., 11, 309–317, 1954. 7509
Bony, S. and Dufresne, J.-L.: Marine boundary layer clouds at the heart of tropical cloud feedback uncertainties in climate models, Geophys. Res. Lett., 32, L20806, doi:10.1029/2005GL023851, 2005. 7508
Chiu, J. C., Marshak, A., Knyazikhin, Y., Wiscombe, W. J., Barker, H. W., Barnard, J. C., and Luo, Y.: Remote sensing of cloud properties using ground-based measurements of zenith radiance, J. Geophys. Res., 111, D16201, doi:10.1029/2005JD006843, 2006. 7511, 7516, 7522
Dong, X., Ackerman, T. P., Clothiaux, E. E., Pilewskie, P., and Han, Y.: Microphysical and radiative properties of boundary layer stratiform clouds deduced from ground-based measurements, J. Geophys. Res., 102, 23829–23843, 1997. 7510, 7521
Fox, N. I. and Illingworth, A. J.: The retrieval of stratocumulus cloud properties by ground-based cloud radar, J. Appl. Meteorol., 36, 485–492, 1997. 7509
Frisch, A. S., Fairall, C. W., and Snider, J. B.: Measurement of stratus cloud and drizzle parameters in ASTEX with a Ka-band Doppler radar and a microwave radiometer, J. Atmos. Sci., 52, 2788–2799, 1995. 7509, 7510
Frisch, A. S., Feingold, G., Fairall, C. W., Uttal, T., and Snider, J. B.: On cloud radar and microwave radiometer measurements of stratus cloud liquid water profiles, J. Geophys. Res., 103, 23195–23197, 1998. 7509, 7510, 7511, 7513, 7530, 7533
Frisch, A. S., Martner, B. E., Djalalova, I., and Poellot, M. R.: Comparison of radar/radiometer retrievals of stratus cloud liquid-water content profiles with in situ measurements by aircraft, J. Geophys. Res., 105, 15361–15364, 2000. 7521
Frisch, S., Shupe, M., Djalalova, I., Feingold, G., and Poellot, M.: The retrieval of stratus cloud droplet effective radius with cloud radars, J. Atmos. Ocean. Tech., 19, 835–842, 2002. 7509
Kato, S., Mace, G. G., Clothiaux, E. E., Liljegren, J. C., and Austin, R. T.: Doppler cloud radar derived drop size distributions in liquid water stratus clouds, J. Atmos. Sci., 58, 2895–2911, 2001. 7509
Kim, B.-G., Schwartz, S. E., Miller, M. A., and Min, Q.: Effective radius of cloud droplets by ground-based remote sensing: relationship to aerosol, J. Geophys. Res., 108, 4740, doi:10.1029/2003JD003721, 2003. 7518
Kim, B.-G., Miller, M. A., Schwartz, S. E., Liu, Y., and Min, Q.: The role of adiabaticity in the aerosol first indirect effect, J. Geophys. Res., 113, D05210, doi:10.1029/2007JD008961, 2008. 7510

AMTD
5, 7507–7533, 2012

Klein, S. A. and Hartmann, D. L.: The seasonal cycle of low stratiform clouds, J. Climate, 6, 1587–1606, 1993. 7508
Kogan, Y. L., Kogan, Z. N., and Mechem, D. B.: Assessing the errors of cloud liquid water and precipitation flux retrievals in marine stratocumulus based on Doppler radar parameters, J. Hydrometeorol., 8, 665–677, doi:10.1175/JHM603.1, 2007. 7509
Kollias, P., Clothiaux, E. E., Miller, M. A., Albrecht, B. A., Stephens, G. L., and Ackerman, T. P.: Millimeter-wavelength radars: new frontier in atmospheric cloud and precipitation research, B. Am. Meteorol. Soc., 88, 1608–1624, doi:10.1175/BAMS-88-10-1608, 2007. 7521
Kollias, P., Rémillard, J., Luke, E., and Szyrmer, W.: Cloud radar Doppler spectra in drizzling stratiform clouds: 1. Forward modeling and remote sensing applications, J. Geophys. Res., 116, D13201, doi:10.1029/2010JD015237, 2011. 7517
Korolev, A. V. and Mazin, I. P.: Supersaturation of water vapor in clouds, J. Atmos. Sci., 60, 2957–2974, 2003. 7515, 7521, 7522, 7527
Liu, Y., Geerts, B., Miller, M., Daum, P., and McGraw, R.: Threshold radar reflectivity for drizzling clouds, Geophys. Res. Lett., 35, L03807, doi:10.1029/2007GL031201, 2008. 7509
Luke, E. and Kollias, P.: Separating cloud and drizzle radar moments during precipitation onset using Doppler spectra, J. Atmos. Ocean. Tech., in review, 2012. 7517
Mace, G. G. and Sassen, K.: A constrained algorithm for retrieval of stratocumulus cloud properties using solar radiation, microwave radiometer, and millimeter cloud radar data, J. Geophys. Res., 105, 29099–29108, 2000. 7510, 7521
Martucci, G. and O'Dowd, C. D.: Ground-based retrieval of continental and marine warm cloud microphysics, Atmos. Meas. Tech., 4, 2749–2765, doi:10.5194/amt-4-2749-2011, 2011. 7510
Matrosov, S. Y., Uttal, T., and Hazen, D. A.: Evaluation of radar reflectivity-based estimates of water content in stratiform marine clouds, J. Appl. Meteorol., 43, 405–419, 2004. 7511
McComiskey, A., Feingold, G., Frisch, A. S., Turner, D. D., Miller, M. A., Chiu, J. C., Min, Q., and Ogren, J. A.: An assessment of aerosol-cloud interactions in marine stratus clouds based on surface remote sensing, J. Geophys. Res., 114, D09203, doi:10.1029/2008JD011006, 2009. 7510
Meneghini, R.: Rain-rate estimates for an attenuating radar, Radio Sci., 13, 459–470, doi:10.1029/RS013i003p00459, 1978. 7511
Miles, N. L., Verlinde, J., and Clothiaux, E. E.: Cloud droplet size distributions in low-level stratiform clouds, J. Atmos. Sci., 57, 295–311, 2000. 7513, 7518

AMTD
5, 7507–7533, 2012

Ramanathan, V., Cess, R. D., Harrison, E. F., Minnis, P., Barkstrom, B. R., Ahmad, E., and Hartmann, D.: Cloud-radiative forcing and climate: results from the Earth Radiation Budget Experiment, Science, 243, 57–63, 1989. 7508

Randall, D. A., Coakley Jr., J. A., Fairall, C. W., Kropfli, R. A., and Lenschow, D. H.: Outlook for research on subtropical marine stratiform clouds, B. Am. Meteorol. Soc., 65, 1290–1301, 1984. 7508

Rémillard, J., Kollias, P., Luke, E., and Wood, R.: Marine boundary layer cloud observations in the Azores, J. Climate, doi:10.1175/JCLI-D-11-00610.1, in press, 2012. 7518

Rogers, R. R. and Yau, M. K.: A Short Course in Cloud Physics, 3rd Edn., International Series in Natural Philosophy, Vol. 113, Butterworth Heinemann, Burlington, MA, 1989. 7514

Sassen, K. and Liao, L.: Estimation of cloud content by W-band radar, J. Appl. Meteorol., 35, 932–938, 1996. 7509

Sauvageot, H. and Omar, J.: Radar reflectivity of cumulus clouds, J. Atmos. Ocean. Tech., 4, 264–272, 1987. 7509

Stevens, B. and Feingold, G.: Untangling aerosol effects on clouds and precipitation in a buffered system, Nature, 461, 607–613, doi:10.1038/nature08281, 2009. 7508

Turner, D. D., Vogelmann, A. M., Austin, R. T., Barnard, J. C., Cady-Pereira, K., Chiu, J. C., Clough, S. A., Flynn, C., Khaiyer, M. M., Liljegren, J., Johnson, K., Lin, B., Long, C., Marshak, A., Matrosov, S. Y., McFarlane, S. A., Miller, M., Min, Q., Minnis, P., O'Hirok, W., Wang, Z., and Wiscombe, W.: Thin liquid water clouds: their importance and our challenge, B. Am. Meteorol. Soc., 88, 177–190, doi:10.1175/BAMS-88-2-177, 2007. 7509, 7511

Twomey, S.: The influence of pollution on the shortwave albedo of clouds, J. Atmos. Sci., 34, 1149–1152, 1977. 7509

Wang, J. and Geerts, B.: Identifying drizzle within marine stratus with W-band radar reflectivity, Atmos. Res., 69, 1–27, doi:10.1016/j.atmosres.2003.08.001, 2003. 7509

Wood, R. and Hartmann, D. L.: Spatial variability of liquid water path in marine low cloud: the importance of mesoscale cellular convection, J. Climate, 19, 1748–1764, 2006. 7511

AMTD
5, 7507–7533, 2012

Table 1. Cloud properties measured or derived from ARM observations in the Azores.

Measured quantity	Variable	Instrument
Radar reflectivity	Z ($\mathrm{mm^6\,m^{-3}}$)	WACR
Cloud top height	h_{TOP} (m)	WACR
Cloud base height	h_{BASE} (m)	Ceilometer
Cloud vertical air motion	w_{air} ($\mathrm{m\,s^{-1}}$)	WACR
Cloud liquid water path	LWP ($\mathrm{g\,m^{-2}}$)	MWR
Cloud optical depth	τ_{NFOV}	NFOV

AMTD
5, 7507–7533, 2012

Table A1. List of expressions used throughout this work, but left undefined, and some symbols (adapted from Korolev and Mazin, 2003).

Symbol	Description	Units
S_{qs}	$\frac{a_0 w_{air}[F_k+F_D]}{b_0 N_{cld} r_0 \exp(\sigma^2/2)}$	–
a_0	$\frac{g}{R_m T}\left(\frac{L_v R_m}{c_{pm} R_v T}-1\right)$	m^{-1}
b_0	$\frac{4\pi\rho_w}{\rho_a}\left(\frac{1}{q_v}+\frac{L_v^2}{c_{pm} R_v T^2}\right)$	–
F_k	$\left(\frac{L_v}{R_v T}-1\right)\frac{\rho_w L_v}{KT}$	$m^2 s^{-1}$
F_D	$\frac{\rho_w R_v T}{e_s(T) D}$	$m^2 s^{-1}$
c_{pm}	Specific heat capacity of moist air at constant pressure	$J kg^{-1} K^{-1}$
D	Coefficient of water vapour diffusion in the air	$m^2 s^{-1}$
$e_s(T)$	Saturation vapour pressure over water	Pa
g	Acceleration of gravity	$m s^{-2}$
K	Coefficient of air heat conductivity	$J m^{-1} s^{-1} K^{-1}$
L_v	Latent heat for liquid water evaporation	$J kg^{-1}$
q_v	Water vapour mixing ratio	–
R_m	Specific gas constant of moist air	$J kg^{-1} K^{-1}$
R_v	Specific gas constant of water vapour	$J kg^{-1} K^{-1}$
T	Temperature	K
w_{air}	Vertical air motion	$m s^{-1}$
ρ_a	Density of dry air	$kg m^{-3}$
ρ_w	Density of liquid water	$kg m^{-3}$

AMTD
5, 7507–7533, 2012

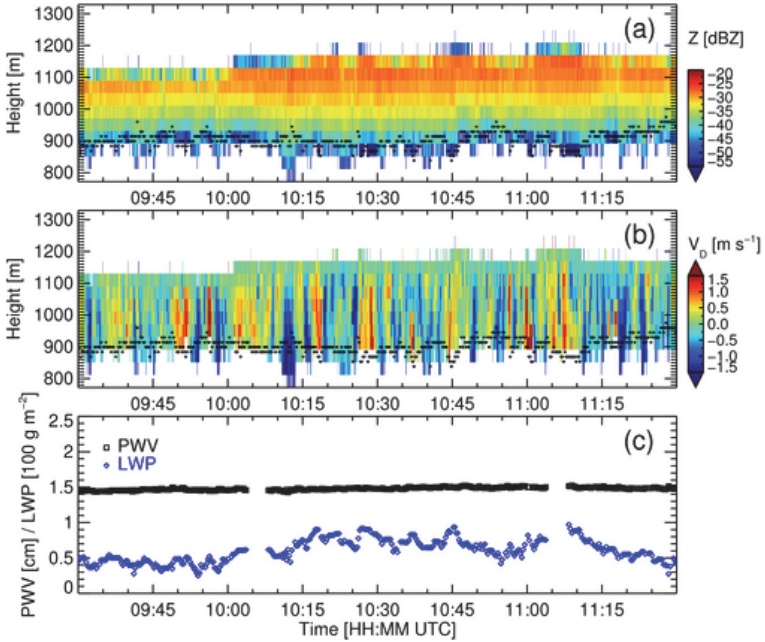

Fig. 1. Measurements made over a two-hour period on 13 June 2010: **(a)** radar reflectivity factor, **(b)** mean Doppler velocity (positive values indicate upward motion), and **(c)** LWP (blue) and PWV (black) from the MWR. The black dots in **(a, b)** represent the cloud-base height as measured by the ceilometer.

AMTD
5, 7507–7533, 2012

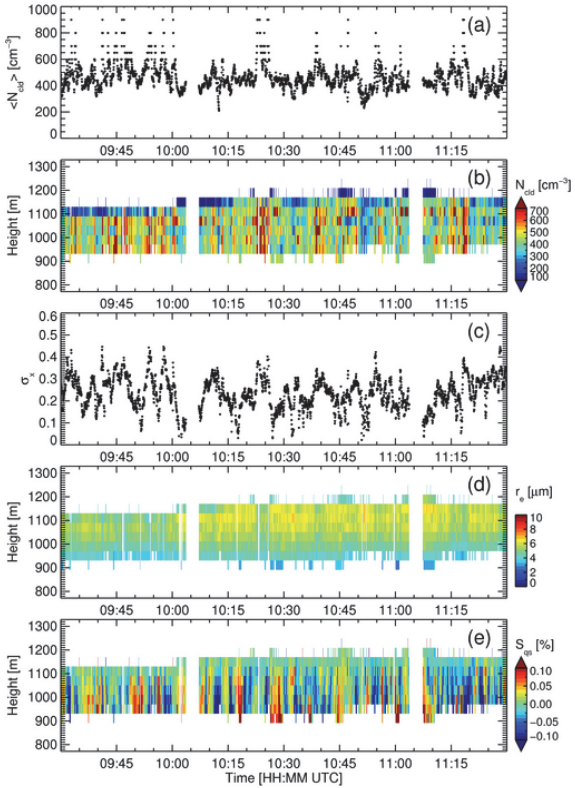

Fig. 2. Microphysical retrievals obtained over two hours on 13 June 2010: **(a)** column-averaged cloud droplet number concentration $\langle N_{cld} \rangle$, **(b)** vertical profile of cloud droplet number concentration $N_{cld}(z)$, **(c)** logarithmic width σ, **(d)** cloud effective radius profile $r_e(z)$, and **(e)** supersaturation profile $S_{qs}(z)$. Periods without retrievals are associated with missing MWR retrievals, or failure of reaching a minimum in Eq. (15).

AMTD
5, 7507–7533, 2012

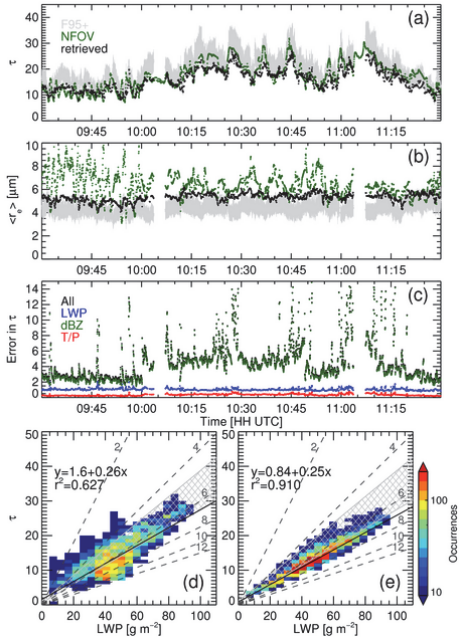

Fig. 3. Comparison results for two hours on 13 June 2010: **(a)** cloud optical depth τ, and **(b)** cloud-layer averaged effective radius $\langle r_e \rangle$, as computed from the retrieved PSD parameters (black), and as retrieved from the NFOV and LWP measurements (green). **(c)** Errors in the retrieved optical depth, evaluated from the propagation of errors from each instrument and overall. The lower scatter plots show the relationship of τ as a function of the LWP values, as obtained **(d)** by the NFOV or **(e)** from the method described here. The black line represents the linear regression performed on the data (excluding those where LWP $< 20\,\mathrm{g\,m^{-2}}$), with its equation and the goodness of the fit reported in the legend. The dashed lines depict the slopes expected for different values of $\langle r_e \rangle$. The grey shaded or hatched regions illustrate the range of results obtained when using the F95+ method with σ varied between 0.2 and 0.46 (the upper limit is the value reported by Frisch et al., 1998).

AMTD
5, 7507–7533, 2012

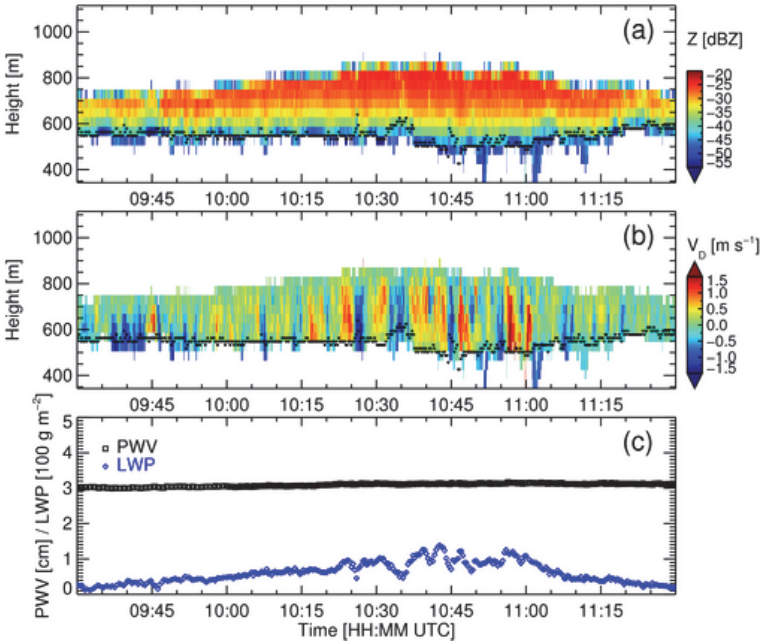

Fig. 4. Measurements made over a two-hour period on 29 June 2010: **(a)** radar reflectivity factor, **(b)** mean Doppler velocity (positive values indicate upward motion), and **(c)** LWP (blue) and PWV (black) from the MWR. The black dots in **(a, b)** represent the cloud-base height as measured by the ceilometer.

AMTD
5, 7507–7533, 2012

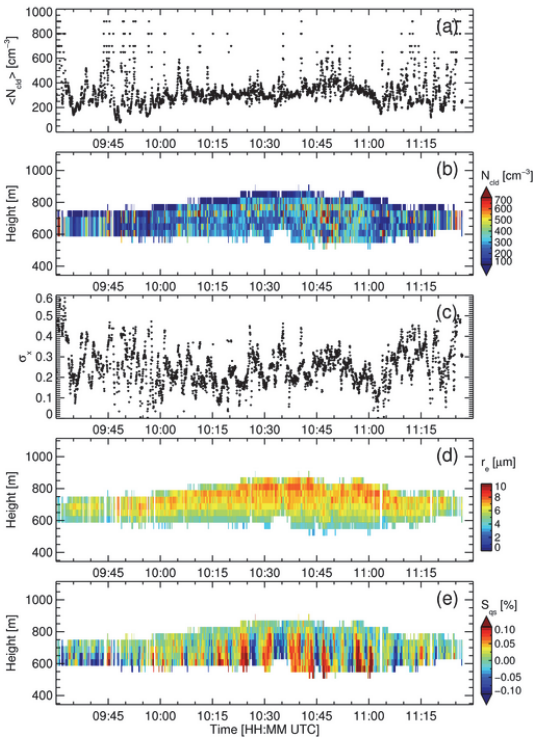

Fig. 5. Microphysical retrievals obtained over two hours on 29 June 2010: **(a)** column-averaged cloud droplet number concentration $\langle N_{cld} \rangle$, **(b)** vertical profile of cloud droplet number concentration $N_{cld}(z)$, **(c)** logarithmic width σ, **(d)** cloud effective radius profile $r_e(z)$, and **(e)** supersaturation profile $S_{qs}(z)$. Periods without retrievals are associated with missing MWR retrievals, or failure of reaching a minimum in Eq. (15).

AMTD
5, 7507–7533, 2012

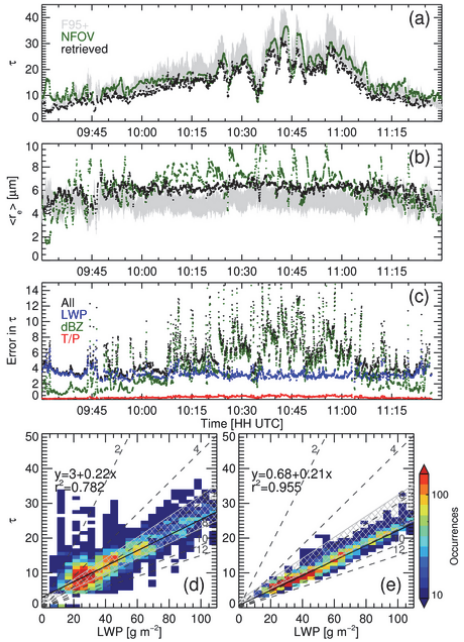

Fig. 6. Comparison results for two hours on 29 June 2010: **(a)** cloud optical depth τ, and **(b)** cloud-layer averaged effective radius $\langle r_e \rangle$, as computed from the retrieved PSD parameters (black), and as retrieved from the NFOV and LWP measurements (green). **(c)** Errors in the retrieved optical depth, evaluated from the propagation of errors from each instrument and overall. The lower scatter plots show the relationship of τ as a function of the LWP values, as obtained **(d)** by the NFOV or **(e)** from the method described here. The black line represents the linear regression performed on the data (excluding those where LWP $< 20\,\mathrm{g\,m^{-2}}$), with its equation and the goodness of the fit reported in the legend. The dashed lines depict the slopes expected for different values of $\langle r_e \rangle$. The grey shaded or hatched regions illustrate the range of results obtained when using the F95+ method with σ varied between 0.2 and 0.46 (the upper limit is the value reported by Frisch et al., 1998).

AMTD
5, 7507–7533, 2012